JOURNAL OF CATALYSIS 127, 576–594 (1991)

Nickel-Catalyzed Methanation Reactions Studied with an *in Situ* Magnetic Induction Method: Experiments and Modeling

PETER W. YESGAR* AND MOSHE SHEINTUCH

Departments of Chemical Engineering, Technion-Israel Institute of Technology, Haifa 32000, Israel

Received May 18, 1990; revised September 18, 1990

Methanation reactions of CO or CO_2 catalyzed by a commercial Ni/kiesel-guhr catalyst, and the adsorption of the relevant reactants and products, were studied with an *in situ* magnetic induction method using a low-field ac permeameter. At the conditions studied, CH_4 was the only product observed and both reactions exhibited similar rates and trends. Comparison of the magnetic data under reaction to the individual contributions expected from adsorption suggests that adsorbed CO was the dominant surface species in CO methanation, while adsorbed CH_4 was the dominant species in CO_2 methanation. The reaction rate and relative magnetic loss were modeled using parameters obtained from single-species magnetic-adsorption data. Adsorptions were modeled with a Langmuir-type isotherm. Rates of methanation were successfully described by a Langmuir—Hinshelwood rate expression using the single-species adsorption parameters and extracting the surface-reaction rate constant. The magnetic loss was predicted then, using predetermined parameters, and compared to observations. Adequate prediction was observed for CO_2 methanation whereas significant deviation exists for CO methanation. The latter result is due to the falsification of CO and possibly CH_4 adsorption parameters by irreversible processes.

INTRODUCTION

Determination of actual reaction mechanisms invariably requires knowledge of the physicochemical behavior of reactive species and of the catalyst during reaction. The application of *in situ* experimental techniques enables one to obtain such information directly, as opposed to indirect information based on a mechanism that yields a rate equation which describes the results statistically. Ideally, one wants to obtain *in situ* data at conditions for which the particular reaction is to be of practical use. Unfortunately, however, successful application of most *in situ* techniques of surface science requires performing experiments under controlled conditions (e.g., high vacuum, with well-defined, single-crystal metal surfaces) which are not typical of commercial catalytic processes. Infrared spectroscopy (IR), solid electrolyte potentiometry (SEP), contact potential difference (CPD), Mossbauer Spectroscopy, X-ray techniques, and magnetic induction methods are common surface science techniques which can be applied at non-vacuum reactor conditions. Magnetic induction methods are particularly suitable for the *in situ* study of practical catalytic phenomena, since catalysts can be studied in their natural working state; methods of IR, SEP, and CPD require the use of special catalyst preparations (compressed disks of catalyst material, or thin metal films). Magnetic induction methods are ordinarily used for studying processes with Fe, Co, or Ni-based catalysts. These metals are widely employed as components of catalysts in commercial hydrotreating processes.

The main objective of this study is to investigate and compare the *in situ* behavior of CO and CO_2 methanation catalyzed by Ni/kieselguhr, under atmospheric pressure, by using a low-field ac magnetic-induction method. For each reaction *in situ* changes

* Currently with Union Carbide, Territown Technical Center, Territown, New York.

0021-9517/91 $3.00

in catalyst magnetization will be related to the gas-phase composition, to the attained reaction rate, and to the expected individual contributions due to adsorption on the catalyst. That will enable us to identify the dominant surface species. Another objective of this work is to present a practical method for incorporating this information in the kinetic modeling. The *in situ* magnetic-adsorption data of individual components will provide adsorption parameters to be used in the rate expression. The measured reaction rates are then fitted with an expression having a single adjustable parameter. The measured magnetic-reaction data now can be compared (with no adjustment) to the prediction of the rate expression and the adsorption isotherms.

Application of the magnetic-induction method to the study of catalytic processes on supported metal catalysts requires that the catalyst particles exhibit a special form of magnetism which has combined characteristics of ordinary paramagnetism and ferromagnetism. Sufficiently small particles of ferromagnetic material (<500 A, for Ni), when placed in an external field, tend to behave like paramagnetic atoms which have a very large magnetic moment, characteristic of a ferromagnetic. Such particles are said to exhibit *superparamagnetism* (*1*). Interpretation of magnetic data obtained from applying magnetic induction methods is based upon the analysis used by Selwood (*2*). At conditions for which the catalyst magnetization, $M(T_i)$, is far from its saturation value and under the assumption that the particles are uniform, the magnetization of a group of N superparamagnetic particles at temperature T_i, each of volume ν_p, can be written as

$$M(T_i) = \frac{N I_s^2(T_i) \nu_p^2 H}{3kT_i}, \qquad (1)$$

where H is the magnetic field, $I_s(T_i)$ is the spontaneous magnetization (sometimes called the saturation magnetization) of the catalyst, and k is Boltzmann's constant. As a result of the chemisorption process, the magnetic moment of a given particle, $I_s\nu_p$, changes by $\Delta\mu$, and the relative change in magnetization for the catalyst is written as

$$\frac{\Delta M}{M} = \frac{-2\Delta\mu}{I_s\nu_p} + \left(\frac{\Delta\mu}{I_s\nu_p}\right)^2. \qquad (2)$$

Thus, by monitoring the relative change in catalyst magnetization, one can obtain *in situ* information on the change in the chemisorbed state of the catalyst.

The surface behavior of many commercially important absorbates, on Ni/SiO_2 or Ni/kieselguhr catalysts, has been successfully investigated by employing in situ magnetic induction methods. The interaction of hydrogen with adsorbed species is sometimes discussed in these adsorption studies. However, few studies have applied the magnetic induction method specifically for investigating nickel catalyzed hydrogenation reactions. Van Meerten *et al.* (*3*) studied the structure sensitivity and crystallite size change of nickel during CO methanation on Ni/SiO_2 catalysts, using low-field magnetic induction techniques; an earlier study (*4*) focused attention on the gas-phase hydrogenation and adsorption of benzene and its hydrogenation products. The methanations of CO and CO_2 were studied (*5, 6*), by employing especially prepared nickel catalysts and high-field magnetic-induction techniques. In their studies, a physically consistent rate equation for CO methanation, and a wealth of mechanistic information were obtained from the in situ magnetic data. A low-field ac permeameter was used by Cale (*7*), for studying nickel crystallite thermometry during hydrogenolysis of C_2H_6.

EXPERIMENTAL

Apparatus

Reactor system. Adsorption and hydrogenation studies were performed with a laboratory scale, continuous flow, fixed bed, catalytic reactor system. The feed gases (hydrogen, carbon monoxide, carbon dioxide, methane, oxygen, and helium), each having a purity better than 99.9%, were sup-

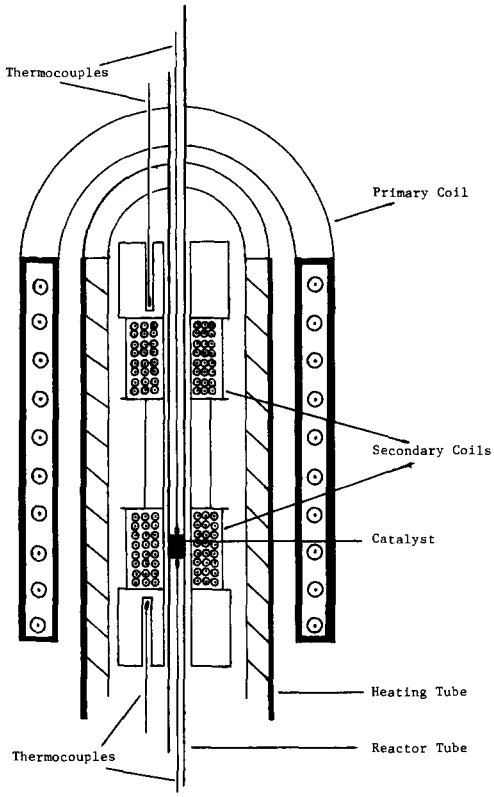

FIG. 1. Detail view of the reactor/magnetic system.

plied from regulated cylinders. An electronic mass flow control system (Brooks, model 5878) was used for precise control of volumetric flow rates. In-line molecular sieves (5 A) drying cylinders and 5-μm filters removed traces of water and any particulates from the feed gases. Deoxo units were connected to the hydrogen and helium lines. An auxiallary helium feed system was used for purging and maintaining the catalyst in an inert environment. The reactor was a 3.86-mm-i.d. stainless-steel tube, 40 cm in length, mounted vertically (Fig. 1). The catalyst bed (about 0.23 cm^3) consisted of a 0.60-gram sample of Ni/kieselguhr particles. Reaction gas flowed downward through the catalyst bed, which was supported by a thin layer of Pyrex glass wool. The reactor heater, an aluminum tube (2.8-cm i.d. and 30-cm length), wrapped with cylindrical windings of thin nichrome wire sandwiched between layers of asbestos, was manually controlled with a variac. Process thermocouples (Type K) were used to measure the temperatures of entering and exiting gas, as well as the top and bottom of the catalyst bed. Precision shut-off valve, positioned upstream from the reactor inlet, enabled diversion of the feed and bypass of the reactor for sampling and chemical analysis. A heating tape was wrapped around the outlet line; this prevented condensation of water in the reactor effluent. The outlet line was directly connected to the mass spectrometer.

Catalyst. The commercial Ni/kieselguhr catalyst (Harshaw Chemicals, Ni-6458 T) contained about 60% nickel in its reduced form and had a BET surface area of 150 m^2/g. X-ray diffraction line-broadening analysis of the reduced catalyst showed that the average Ni crystallite diameter was 17.5 nm. The Scherrer equation was used for evaluating the X-ray diffraction data, with a Cu$K\alpha$ X-ray wavelength of 0.1542 nm and a Scherrer constant of 0.90 (*8*). Catalyst tablets were crushed and sieved to 0.23-mm average diameter before charging to the reactor. Several charges of 0.60-g catalyst were used throughout the study.

AC magnetic permeameter. In situ magnetic measurements were performed with a magnetic permeameter especially built around the reactor system (Fig. 1). The primary coil consisted of about 3500 turns of polyvinyl insulated copper wire (1.5-mm diam), wound on an asbestos core 5.2-cm i.d. and 12.0 cm long. Power to the primary coil was supplied by a variable function regulated ac power supply, with a step-up voltage transformer included in the circuit. The primary coil was operated with a current of 2.15 A and a frequency of 160 Hz. The current was sufficiently low as not to require a special cooling system around the coil, and the frequency was high enough for stable input current and noninterference from mainline frequency (50–60 Hz). At these conditions, superparamagnetic behavior

was observed for the catalyst samples. Two secondary coils compactly fitted around the tubular reactor and inside the reactor heater. The catalyst bed was at the center of the lower secondary coil; the upper coil surrounded the empty reactor tube as a reference. Each coil, 3.5 cm long, consisting of about 2800 turns of nonmagnetic chromium alloy wire (0.025 cm) with glass braid insulation, was wound onto a single, precision-machined brass form (2.8-cm o.d., 17.8 cm long). The outer winding of each coil was protected with a thin wrapping of mica, firmly held by thin copper bands. The brass form contained narrow channels filled with ceramic tubing for the purpose of guiding secondary coil thermocouple wires. The secondary coils were connected in opposition, whereby the net secondary output depended only on the difference in magnetic permeability between the materials surrounded by the coils. The secondary coil system could be operated consistently at temperatures up to 700 K. The net output of the secondary coils was fed into an ac to dc rectifier/amplifier device. High- and low-pass electronic filters in the circuit-enhanced stability and accuracy of the output signal. The treated output was read on a digital multi-meter (Keithley, model 175 AMM).

Analytical system. A quadrupole mass spectrometer (Balzers, QMG 511) was employed for analysis of reactor feed and effluent. Once inside the mass analyzer, analysis time for a sample was of the order of seconds. This rapid analysis time was critically important for synchronization of the kinetic and magnetic data. The mass analyzer contained a tungsten–rhenium filament operating at an ionization potential of 70 eV. Vacuum conditions in the mass spectrometer were maintained by a coordinated multiple pumping system, including a turbomolecular pump. The pressure in the vacuum chamber was measured with a hot cathode (thoriated iridium) Bayard–Alpert ionization gauge. Reactor effluent was continuously fed into the mass spectrometer via a heated stainless-steel capillary tube. Reproducible analytical conditions were maintained by baking out the vacuum chamber and its contents, prior to each hydrogenation or adsorption series, and by outgassing the ionization filaments at a current high enough to burn off chemical deposits (primarily carbon). Calibration and determination of sensitivity factors of the particular compounds under study were routinely performed.

Procedures

Catalyst reduction. A standard catalyst reduction procedure was used to maintain the nickel catalyst active for the kinetic and magnetic experiments. While under a He stream, the catalyst was gradually heated from room temperature to 673 K, in 2 h. It then was held at 673 K for 1 h and then cooled to room temperature. A series of He/H_2 mixtures with increasing H_2 content was vented through the reactor. Pure H_2 was then passed through the reactor, which was at about 120 kPa. After 30 min at room temperature, the reactor was gradually heated to 673 K in 2 h held at 673 K for at least 15 h, and was cooled to 403 K. Finally, the H_2 purge was replaced by a He purge. A large increase in catalyst magnetization (secondary coil output), following the reduction procedure, indicated that the catalyst had reached its magnetically and catalytically active state.

Thermal characterization of the reactor/magnetic system. As kinetic and magnetic measurements are sensitive functions of temperature, it was necessary to investigate the thermal characteristics of the reactor/magnetic system. During a typical experiment, catalyst temperatures at the top and bottom of the catalyst bed were measured, while secondary coil temperatures were monitored with junctions embedded near the coil wrappings (see Fig. 1). Additional experiments were performed, to determine temperature gradients along the bed, by changing the vertical position of the thermo-

couple junctions along the reactor tube during reaction. The temperature distribution was first measured with preadsorbed H_2 before admission of the second reactant. Prior to reaction certain gradients existed throughout the reactor/magnetic system due to its physical configuration and the initial flow of hydrogen. Thereafter, temperatures were recorded when the reaction reached steady state. Catalyst top temperature was maintained constant; it was used as the reference temperature throughout the reaction studies. Temperature gradients under reaction ordinarily increased as a result of the exothermicity of the reaction and it was necessary to decrease the heat supplied to the reactor via the externally controlled tubular heater. For example, at 573 K, the longitudinal thermal gradient (along the catalyst bed) reached about 15°. The gradient due to reaction, however, was usually less than 5°. The temperature difference between the secondary coils was always less than 5°, and remained essentially constant before and during reaction.

Methanation reactions. Prior to each methanation run the catalyst was reduced in H_2, cleaned with He, and then cooled to initial reaction temperature. The catalyst was then brought to a steady state with adsorbed H_2. In a typical run the reactant concentration was increased, by steps of 0.5 vol%, up to 5.0 vol% and then decreased again in order to search for possible instabilities (e.g., hysteresis) and to test for experimental reproducibility. Steady state was maintained for at least 30 min before reaction data was recorded. For the conditions employed in this study, it was determined that heat and mass transport limitations were not significant and the results represent intrinsic kinetics (*9*).

Adsorption studies. The adsorption properties of single components were determined from the change in catalyst magnetization as a function of gas-phase concentration in He, while maintaining a constant total pressure. Prior to each adsorption experiment the catalyst was reduced, hydrogen was then purged from the reactor with He flow and the reactor was cooled to a constant temperature. Adsorbate/He mixtures were introduced to the catalyst. After each change in composition, at least 15 min were given for attainment of steady state. Secondary coil output, catalyst, and secondary coil temperatures were then recorded. At the end of each run pure He was flowed though the reactor and the recovery of catalyst magnetization, at constant temperature, was recorded. At the end of every sequence, the catalyst was heated in either pure He or in mixtures of H_2 and He, while monitoring the desorption products with the mass spectrometer. To assure uniformity in comparing the results, a new catalyst sample (from the same batch) was used for each adsorbate. Catalyst magnetization was periodically measured as a function of temperature, in flowing He or H_2, between adsorption experiments. This served as a direct check on the magnetic activity of the catalyst.

Catalyst activity. Catalyst activity was monitored in two ways: kinetic and magnetic. For each catalyst sample, kinetic activity was monitored by periodically repeating methanation or adsorption experiments. Magnetic activity was monitored by measuring the magnetization as a function of temperature, before and after methanation or adsorption runs, while the catalyst was under He flow. Variation of catalyst activity with exposure time (not including periods between runs when the catalyst was exposed to pure He at about 420 K) was strongly dependent on the particular methanation conditions used. Reproducible activity, during the methanation reactions, was reached after about 20 to 30 exposure hours. Steady-state concentration and magnetic output were sufficiently reproducible then to justify the use of average values in the data analysis. At least five methanation runs (about 85 h) were performed before irreversible deactivation had been ob-

served; thereupon, the catalyst sample was replaced.

Methodology of the Magnetic Measurements

The magnetic behavior of the catalyst was characterized in order to determine the approximate deviation from ideal superparamagnetic behavior and in order to determine the temperature dependence of the spontaneous magnetization, $I_s(T_i)$, in Eq. (1). In this study, the low-field approximation to the Langevin function was employed, since the maximum field strength produced by the primary coil was calculated to be less than 0.1 T (*9*). Evidence for superparamagnetic behavior of the catalyst, in the reduced state and when exposed to He flow, was tested against two criteria.

The first criterion is a linear relationship between the secondary coil output (catalyst magnetization) and primary coil current (applied magnetic field). This dependence was measured at different frequencies of the applied current (40–180 Hz) and for several catalyst temperatures and good agreement was observed. Values of secondary coil output were corrected for by subtracting the background voltage obtained for the reactor system when glass beads were substituted for a catalyst sample. The secondary coil output was also measured as a function of catalyst temperature at constant magnetic field. The catalyst magnetization dropped with increasing temperature. Above 450 K, the nonlinearity in the temperature dependence became significant, illustrating that spontaneous magnetization of the nickel catalyst was inversely proportional to temperature.

The second criterion of superparamagnetism is that the magnetization obtained at different temperatures should superimpose if plotted with respect to H/T (primary coil current divided by absolute temperature), after accounting for the change of spontaneous magnetization, I_s, with temperature. In this study, saturation magnetizations were not measured, and since values of $I_s(T_i)$ for bulk nickel are not necessarily equivalent to those for a particular nickel catalyst under study (*10*), a normalization procedure was necessary to account for the temperature dependence of the spontaneous magnetization. The procedure is based on a method used by Cale *et al.* (*10*), in which relative magnetic moments are calculated from low-field magnetic data, without having to determine absolute values of $I_s(T_i)$ or catalyst magnetic volume. We can define the relative magnetic moment, γ, at temperature T_i, with respect to a constant reference temperature T_r, as

$$\gamma(T_i, T_r) = \frac{I_s(T_i)}{I_s(T_r)}. \tag{3}$$

Combination of Eq. (1) and (3) gives

$$\frac{M(T_i)}{\gamma^2(T_i, T_r)} = \frac{NI_s^2(T_r)\nu_p^2 H}{3kT_i}. \tag{4}$$

Therefore, we can define normalized magnetization as

$$M(T_i), \text{ normalized} = \frac{M(T_i), \text{ observed}}{\gamma^2(T_i, T_r)}. \tag{5}$$

From Eq. (1), it follows that

$$\gamma(T_i, T_r) = \frac{I_s(T_i)}{I_s(T_r)} = \left(\frac{T_i M(T_i)}{T_r M(T_r)}\right)^{1/2}. \tag{6}$$

This gives an expression for $\gamma(T_i, T_r)$ in terms of temperature and magnetization, once a reference temperature is chosen. The data of the secondary coil output (observed) as a function of absolute temperature were used in calculating values of $\gamma(T_i, T_r)$ for the temperature range used in this study (Table 1). A constant reference temperature of 308 K was chosen for use in the analysis of the magnetic data.

Having determined the temperature dependence of the spontaneous magnetization, the magnetic data can now be tested for the criterion of superposition, by plotting the normalized catalyst magnetization

TABLE 1

Values of the Relative Magnetic Moment as a Function of Temperature

Temp. (K)	308	343	403	453	473	493	523	573
$\gamma(T_i, T_{308})$	1.00	0.94	0.85	0.77	0.74	0.70	0.59	0.39

against I/T (Fig. 2). In the figure the magnetic data points measured at 308 K are the reference values, whereas the data obtained at 573 K represents the highest temperature employed and better agreement was obtained at lower temperatures.

An independent check on the temperature behavior of the catalyst magnetization was done by comparing values of the relative magnetic moment, $\gamma(T_i, T_r)$, obtained for the Ni/kieselguhr catalyst, with those for bulk nickel. Relative magnetic moments for bulk nickel were calculated from an experimentally determined plot of spontaneous magnetization as a function of temperature, available in the literature (*11*). Values of $\gamma(T_i, 308\ \text{K})$ are shown plotted as a function of reduced temperature, T_i/T_c, where T_c is the Curie temperature (Fig. 3). The Curie temperature for ordinary bulk nickel, 631 K, need not necessarily apply for the Ni/kieselguhr catalyst used here. Values of the relative magnetic moment for the nickel catalyst were always slightly less than those for bulk nickel and the curves show a similar trend. This deviation is expected for superparamagnetic nickel particles, because their Curie temperature is often less than that of bulk phase ferromagnetic nickel. The curves in Fig. 3 would approximately overlap if a T_c somewhat less than 631 K were used as a reference in the reduced temperature.

Characterization of the magnetic behavior of the catalyst is standard procedure in nearly every catalytic study in which the

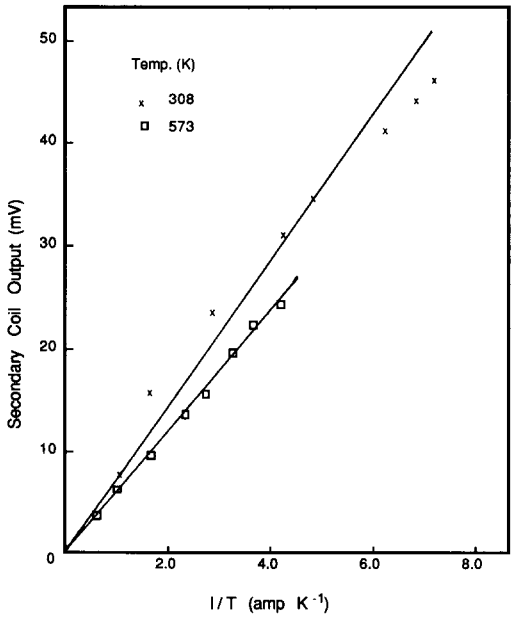

FIG. 2. Confirming the superparamagnetic behavior of the Ni/kieselguhr catalyst. The data shows linear dependence on primary coil current (I) and superposition of I/T. Data at 308 K are the reference values while measurements at 573 K were normalized by using Eq. (5).

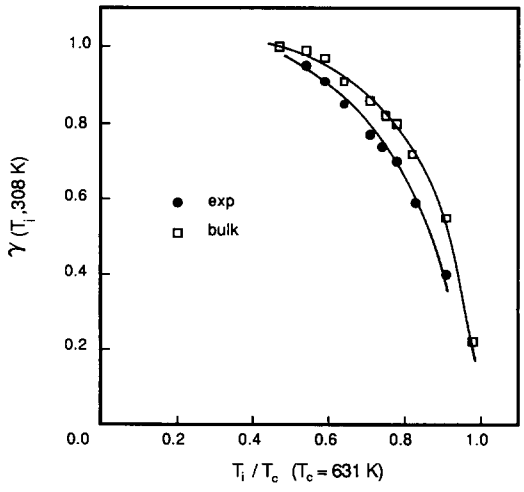

FIG. 3. Relative magnetic moment as a function of reduced temperature for the Ni/kieselguhr catalyst and bulk nickel.

magnetic induction method is applied. The above discussion indicates that the Ni/kieselguhr catalyst satisfied the principal criteria of superparamagnetic behavior for small nickel particles, exposed to the conditions employed in this study.

The normalization procedure can also be applied to Eq. (2) in order to simplify the analysis of the magnetic data. The relative change in catalyst magnetization, at temperature T_i, is to a first-order approximation, inversely proportional to $I_s(T_i)$,

$$\left(\frac{\Delta M}{M}\right)_i, \text{observed} \propto \frac{1}{I_s(T_i)}. \qquad (7)$$

By definition, the normalized relative change in magnetization is the product of these equations,

$$\left(\frac{\Delta M}{M}\right)_i, \text{normalized} = \left(\frac{\Delta M}{M}\right)_i, \text{observed} \cdot \gamma(T_i, T_r). \qquad (8)$$

All experimental values of relative magnetic loss obtained in this study were calculated with this procedure, which enabled comparisons to be made of magnetic data obtained at different catalyst temperatures. Therefore, the *in situ* magnetic data presented in this study are approximately independent of the change in spontaneous magnetization with temperature, and should reflect the physicochemical behavior of the reaction system.

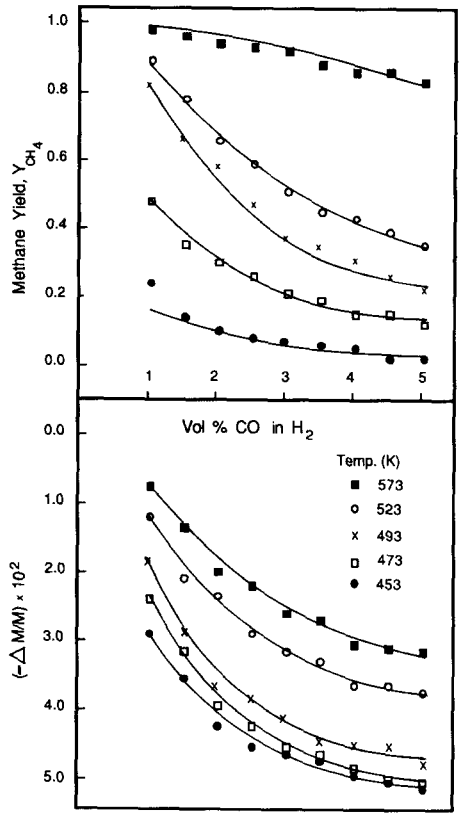

FIG. 4. Yield and magnetic loss during carbon monoxide hydrogenation at 453–573 K, and 120 kPa total pressure. Yield curves are computed with Eq. (20). Magnetic-loss curves are plotted to guide the eye (see modeling in Fig. 12).

RESULTS

Reactions

The dependence of methane yield and relative loss in catalyst magnetization (corrected for the temperature dependence of spontaneous magnetization) on reactant feed concentration and on catalyst temperature (453–573 K) is shown in Figs. 4 and 5, for CO and CO_2 methanations, respectively. Magnetic loss values are the difference between the recorded values under reaction and the reference state of H_2 adsorption. Thus, they represent the change in magnetic state due to reaction. Methane and water were the only significant products, under these conditions. At the lower temperature (<473 K), trace amounts of higher hydrocarbons (C_2H_6, C_3H_8) were detected during CO hydrogenation, but were not included in the calculations. Material balance of the various species during reaction was consistent within 5%; the shortage was primarily due to analytical limitations associated with the mass spectrometer.

Methane yield declined with increasing reactant concentration in the feed, showing a similar trend in both methanation reac-

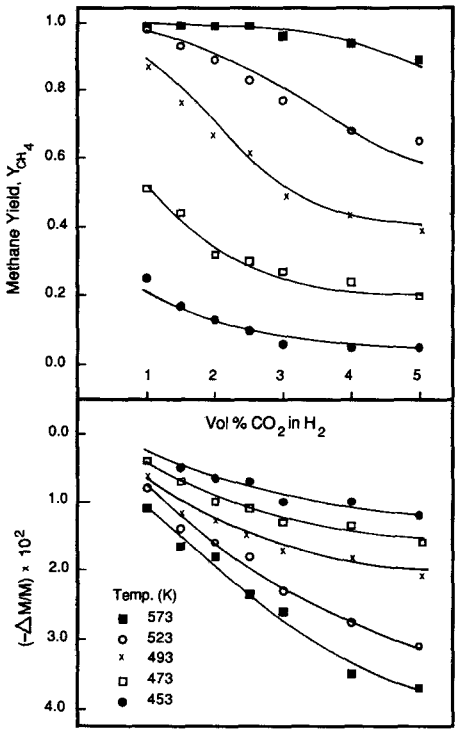

FIG. 5. Yield and magnetic loss during carbon dioxide hydrogenation at 453–573 K, and 120 kPa total pressure. Yield curves are computed with Eq. (20). Magnetic-loss curves are plotted to guide the eye (see modeling in Fig. 12).

tions. Comparison of the data (Figs. 4 and 5) reveals that the effect of reactant inhibition is somewhat smaller in CO_2 methanation. At a given temperature and concentration, CH_4 yields were always large during CO_2 methanation. At 573 K, conversion to CH_4 was essentially complete during CO_2 methanation, except at the higher feed concentrations of CO_2. Relative magnetic loss increased with increasing reactant feed concentration. With increasing temperature the magnetic loss decreased during CO methanation whereas an opposite trend is observed during CO_2 methanation. Magnetic losses during CO_2 methanation, at higher temperatures, were approximately linear over a wider range of feed concentrations. Magnetic losses at low temperatures reached an asymptotic value, similar to the trend observed during CO methanation.

Adsorption Studies

Steady-state magnetization-concentration isotherms for H_2, CO, CO_2, and CH_4 were studied at constant total reactor pressure of 120 kPa, constant total volumetric flow rate of 100 ml/min, in the temperature range of 453 to 573 K. The experimental data, shown in Figs. 6 through 9, represent average values calculated from data of at least three separate isotherm runs for each temperature studied.

Relative magnetic loss decreased with temperature during the adsorption of H_2; for CO, CH_4, and CO_2, magnetic losses increased with increasing temperature. Hydrogen adsorption was reversible; original values of catalyst magnetization were obtained upon reversibly sweeping the concentration of H_2 in He. The results indicate that H_2 adsorption reached apparent ther-

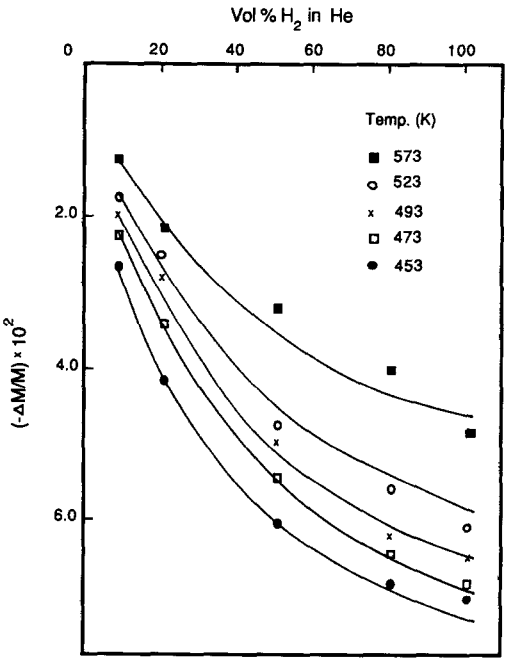

FIG. 6. Hydrogen adsorption isotherms at 120 kPa total pressure.

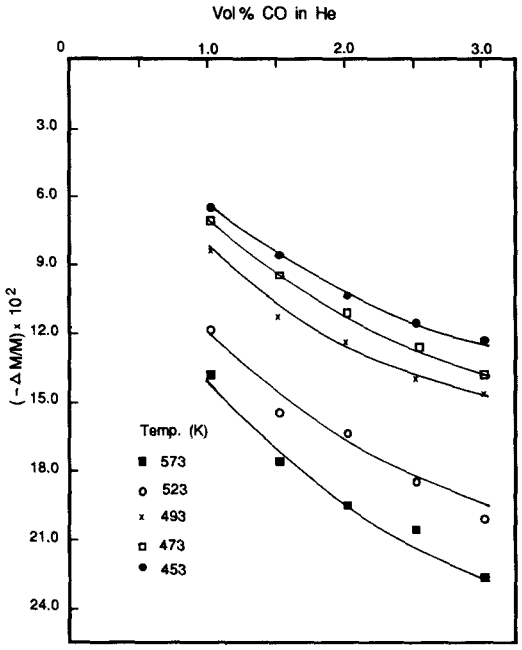

FIG. 7. Carbon monoxide adsorption isotherms at 120 kPa total pressure.

modynamic equilibrium at the catalyst surface. Magnetic loss due to H_2 was significant only at very high concentration. Magnetic losses due to CO and CH_4 adsorption were higher than those due to CO_2, for comparable concentrations. Carbon monoxide and methane adsorptions were found to be slow and irreversible. A time-independent (steady or equilibrium) state is achieved within 30 min. Original levels of catalyst magnetization were not regained upon flowing pure He through the catalyst bed, following the adsorption experiments. In addition, during CO adsorption, small amounts of CO_2 (approximately 1 to 3% of the CO in the feed, increasing with temperature) were observed in the effluent. The results for CO are indicative of disproportionation of CO into C and CO_2 (Boudouard reaction). Carbon dioxide adsorption was irreversible at temperature above 523 K, whereas, for lower temperature, original levels of magnetization were regained after only 30 min of pure He flow. Thus, below 523 K, CO_2 was apparently in adsorption equilibrium. The time required for partial recovery of magnetization during the desorption of CO and CH_4 adsorbed species was significantly higher.

DISCUSSION AND MODELING

Reaction Analysis

The object in this section is to characterize the main features of the methanation reactions by relating the in situ magnetic data to the kinetic data. A consequence of Eq. (2) is that during chemisorption, the relative change in catalyst magnetization is directly proportional to two principal chemisorption parameters, namely, the quantity of adsorbed gas, and the type of adsorbate-Ni bonding configuration. For adsorption of a single gas, under special conditions (using high-field magnetic methods), these parameters can be evaluated separately. During reaction, however, in which reactants and products simultaneously interact with the

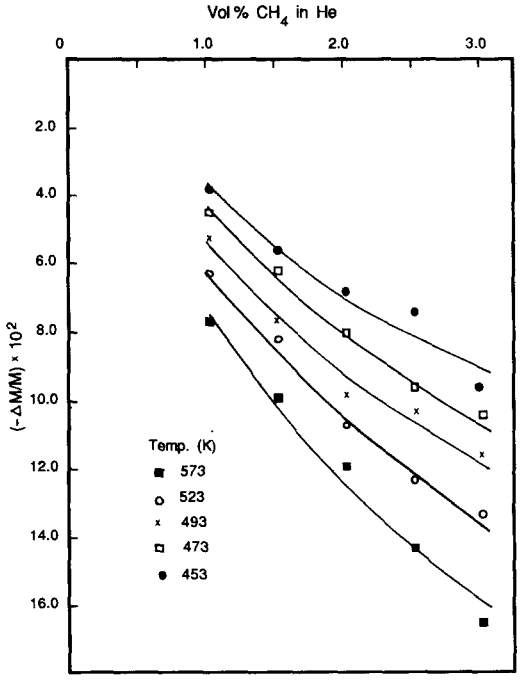

FIG. 8. Methane adsorption isotherms at 120 kPa total pressure.

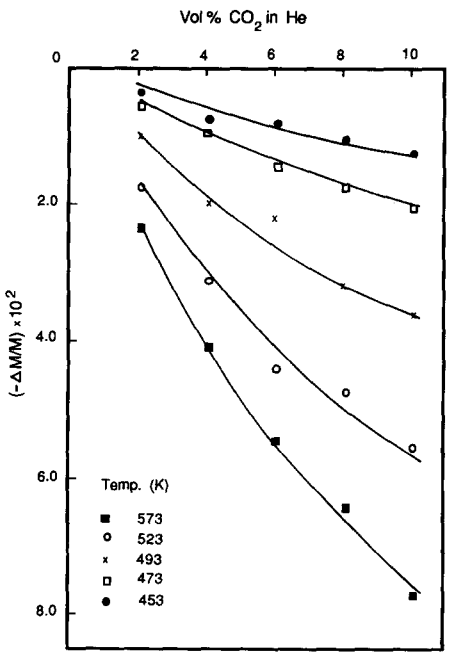

FIG. 9. Carbon dioxide adsorption isotherms at 120 kPa total pressure.

catalyst, $\Delta\mu$ becomes a complex function of the adsorption parameters of the different adsorbates on the surface. Under reaction, the relative change in magnetization can be thought of as reflecting the change in the overall catalyst *surface utilization;* relating the magnetic data to the kinetic data is facilitated by using this term, which roughly represents the combined influence of all the adsorbates on the surface.

To determine the dominant species on the surface during reaction, let us compare the expected contribution of each species to $\Delta M/M$, with that actually observed. Plotted in Fig. 10(a) is the relative magnetic loss versus temperature for a constant (2 vol%) CO feed concentration. This curve was obtained from a cross section of the corresponding data in Fig. 4. Inspection of the figure reveals that as the temperature increased, relative magnetic loss decreased, which corresponded to an increase in CH_4 yield. This result indicates that overall surface utilization decreased with temperature as conversion of CO increased. A similar trend exists for other feed concentrations (Fig. 4). The individual expected adsorption contributions are also plotted (dashed lines), obtained from the magnetization adsorption isotherms of CO and CH_4 (Figs. 6 and 7) at the same temperature and the same partial pressure. The contribution of H_2 was already accounted for, since the reaction data were recorded only after the surface reached steady state with flowing H_2. Adsorption experiments indicated that the contribution due to H_2O was negligibly small.

The magnetic data in Fig. 10(a) indicate that the change in overall surface utilization during methanation was proportional to the expected change in surface utilization for the adsorption of CO. The total expected magnetic loss obtained from the single-gas studies is naturally larger than those for the reaction, since the two species exerted mutual inhibition. This comparison shows that the affinity of the surface for CO was larger for CH_4 and that magnetic loss declines with temperature, even though the partial pressure of CH_4 increases. The relative magnitude of these affinities is already evident from the single species adsorption data (compare Figs. 7 and 8), showing larger magnetic loss for CO than CH_4 under similar conditions. The decline in overall surface utilization during reaction supports the proposal that adsorbed CH_x species apparently accounted for a comparatively small fraction of overall surface utilization. If CH_x constituted the most abundant surface species during methanation, then the trend in overall surface utilization would more likely reflect that by the adsorption of CH_4. This leads to the conclusion that the dominant surface species was CO.

As a comparison, in a study of CO hydrogenation on Ni/SiO_2, Dalmon and Martin (*6*) concluded that a decrease in the saturation magnetization of the catalyst with increasing temperature corresponded to an increase in the conversion of adsorbed CO into gaseous CH_4. In their study they measured changes in saturation magnetization

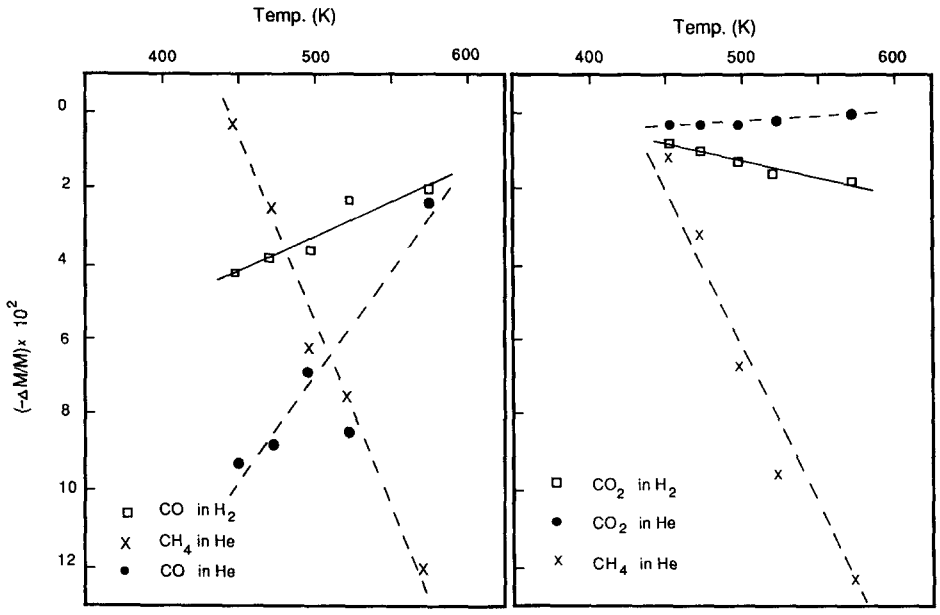

FIG. 10. Determination of the dominant surface species by comparing magnetic loss during reaction of 2 vol% CO (a) or 2 vol% CO_2 (b) with single-species adsorption.

(using high-field magnetic techniques) and observed that, within a certain range, increasing the temperature was accompanied by a decrease in the change of saturation magnetization (directly proportional to the number of occupied Ni sites). The procedures employed in this study for CO methanation and *in situ* magnetic measurements were significantly different from those used in (*6*), but our results are conistent with their interpretation of the magnetic behavior.

Comparison of the kinetic data of Figs. 4 and 5 shows that, although the rates of both carbon oxide methanation reactions are similar, the surface composition under identical condition is significantly different. Plotting the cross section of a given CO_2 methanation magnetization data, as was done for CO, shows increasing overall surface utilization with increasing temperature (Fig. 10(b)). Comparison of the relative magnetic losses observed under reaction with the magnetic losses expected for the individual contributions of CO_2 and CH_4, from their mixture in He, indicates that the surface primarily consisted of CH_x adsorbed species and not of CO_2 species. The large difference in the magnitude of the expected magnetic losses for CO_2 and CH_4 reflects the different affinities of these adsorbates on the Ni surface at nonsaturation conditions (Figs. 7, 8). The single-gas adsorption experiments clearly show that CH_4 utilizes more of the Ni surface than CO_2 for identical reaction conditions.

In the temperature range studied here, Falconer and Zagli (*12*) showed that CO_2 dissociates on Ni/SiO_2 to give CO and O adsorbed species. This result has led to the proposal that the mechanisms of CO_2 and CO methanation are similar. Our results contradict this conclusion, suggesting that either CO_2 dissociation is not immediate or that the formed CO adsorbed species react fast and contribute little to the surface coverage.

Adsorption Analysis

We now correlate from the magnetic data recorded during adsorption with a Lang-

muir-type isotherm and compare our observations with those of previous studies. The relative change in catalyst magnetization was written as

$$\frac{\Delta M}{M} = \frac{-2\Delta\mu}{I_s \nu_p} + \left(\frac{\Delta\mu}{I_s \nu_p}\right)^2. \quad (2)$$

The change in the magnetic moment per particle, $\Delta\mu$, is directly proportional to the amount adsorbed, i.e.,

$$\Delta\mu = x_i m_i, \quad (9)$$

where x_i is the number of molecules of gas i adsorbed on the particle and m_i is the change in the magnetic moment per particle caused by the adsorption of each molecule of gas i (Bohr magneton/molecule). The latter can be expressed as

$$m_i = s_i \mu_B n_B, \quad (10)$$

where s_i is the number of nickel atoms utilized per molecule of species i (sites/molecules), μ_B is the standard Bohr magneton, and n_B is the number of Bohr magnetons per atomic site for nickel. We now have

$$\frac{\Delta M}{M} = \frac{-2\mu_B n_B s_i x_i}{I_s \nu_p} + \left(\frac{\mu_B n_B s_i x_i}{I_s \nu_p}\right)^2 = -2C_m U_i + C_m^2 U_i^2, \quad (11)$$

where

$$C_m = \frac{\mu_B n_B}{I_s \nu_p N} = \frac{\mu_B n_B}{I_s V_p} \quad (12)$$

and

$$U_i = s_i g_i \quad (13)$$

with V_p being the total volume of N catalyst particles of volume ν_p, in the reactor, and

$$g_i = x_i N \quad (14)$$

is equal to the total number of molecules of i adsorbed by the catalyst sample. The magnetic coefficient (site^{-1}), C_m, consists of magnetic constants particular to the catalytic material only, and is independent of any adsorption process. The *surface utilization function*, U_i, for adsorbate i, represents the observed number of nickel atomic sites *utilized* by molecules of i. U_i, having dimensions of number of sites, is expected to be a complex function of temperature and pressure, due to the complex nature of the adsorption parameters, s_i and g_i.

To develop a functional form for U_i in terms of fundamental parameters would necessarily require theoretical knowledge of the adsorption parameters s_i and g_i, for a given adsorbate/catalyst system. For purposes of data analysis, a practical form for U_i is desirable. Clearly, at a constant temperature, as adsorbate pressure increases, a limit is expected to be reached in the amount of catalytic sites utilized by adsorbed molecules of i, possibly corresponding to more than a monolayer coverage. The data suggests representation by a form similar to the Langmuir single species adsorption isotherm, without imposing the assumptions associated with the Langmuir model of chemisorption,

$$U_i = \frac{S_i u_i P_i}{1 + u_i P_i}, \quad (15)$$

where P_i is the partial pressure of gas i in the catalyst bed, S_i is the maximum number of nickel sites utilizable by adsorbed molecules of i at a given temperature, and u_i is being introduced here as the surface utilization coefficient for adsorbate i (dimensions of reciprocal pressure). We can then write Eq. (11) as

$$\frac{\Delta M}{M} = \frac{-2C_m S_i u_i P_i}{1 + u_i P_i} + \left(\frac{C_m S_i u_i P_i}{1 + u_i P_i}\right)^2. \quad (16)$$

By writing the solution to Eq. (16) as

$$\left[1 - \left[1 - \left(\frac{-\Delta M}{M}\right)\right]^{1/2}\right]^{-1} = \left(\frac{1}{C_m S_i u_i}\right)\left(\frac{1}{P_i}\right) + \frac{1}{C_m S_i} \quad (17)$$

and plotting the data in this form, the two parameters $C_m S_i$ and u_i can be determined from the slope $(1/C_m S_i u_i)$ and y-intercept $(1/C_m S_i)$ of the plot for each adsorbate/He

TABLE 2

Surface Utilization Coefficients as a Function of Adsorption Temperature

Temp. (K)	453	473	493	523	573
u_{H_2}(kPa^{-1})	0.033	0.027	0.025	0.024	0.019
u_{CO}(kPa^{-1})	0.24	0.30	0.41	0.056	0.62
u_{CH_4}(kPa^{-1})	0.11	0.13	0.16	0.018	0.23
u_{CO_2}(kPa^{-1})	0.017	0.026	0.048	0.058	0.061
u_{H_2O}(kPa^{-1})	0.027	0.031	0.034	0.039	0.048

system. Good fit is obtained, as is evident from the lines in Figs. 6 through 9, which were plotted by using Eq. (16). Surface utilization coefficients were evaluated and are tabulated as a function of temperature for each gas studied (Table 2).

The surface utilization coefficients reflect the trends observed in the magnetic-adsorption data: u_{H_2} decrease with temperature, whereas u_{CO}, u_{CH_4}, and u_{CO_2} increase with temperature. Surface utilization coefficients for H_2O were calculated indirectly by exploiting the data obtained from O_2 hydrogenation (*9*). Conversion of O_2 was complete within the temperature range studied, suggesting that the adsorbed species consisted mainly of hydrogen and water-like surface intermediates. Relative magnetic loss increased with temperature, indicating an increase in surface utilization with temperature during the formation of water. Although this approach is indirect, the results give a practical in situ approximation to the magnitude of the interaction of H_2O on the Ni/kieselguhr catalyst compared to the other adsorbates. Values of u_{H_2O} are small, of the order of magnitude of u_{H_2}, which implies that surface utilization by H_2O is expected to be minor compared to that by CO and CH_4.

Each of the adsorbates studied in the present work have been previously investigated for their adsorption behavior on Ni/SiO_2 catalysts. The particular behavior of each adsorbate–nickel system depends on the specific properties of the nickel catalyst, and on the reactor conditions employed in the experiments. A detailed discussion for each adsorbate is unnecessary here; however, the main features of adsorption behavior found in this study are briefly discussed with respect to other selected adsorption studies.

A few comments are worthwhile concerning the meaning of the surface utilization coefficient, u_i, defined by Eq. (15). This coefficient should not be thought of as a conventional adsorption coefficient, even though it appears in a Langmuir type of equation for ideal adsorption of a single gas in equilibrium with a catalyst surface. The u_i are directly proportional to two factors: the amount of adsorbate on the surface, and the amount of surface utilized by that amount of adsorbate. The temperature dependence of u_i reflects changes of both factors. Three types of behavior can be categorized (refer to Table 2): (a) If adsorption equilibrium exists and the adsorbate–Ni bond (site) number is temperature independent, then the amount adsorbed decreases with temperature (exothermic adsorption). In this case, u_i is expected to decrease with temperature. This appears to be the case for H_2 adsorption, in which it was observed that the H–Ni bond number is constant within the temperature range studied here (*13*). At these conditions, H_2 normally reaches adsorption equilibrium on Ni/SiO_2 catalysts (*14*). (b) Adsorption equilibrium exists, but the bond number increases with temperature. If the increase in bond number compensates for the decrease in amount adsorbed, then u_i will increase. For CO_2 adsorption at temperatures below 523 K, we concluded that adsorption equilibrium was reached. The bond number of CO_2–Ni was

observed as continuously increasing with temperature in the range of 300 to 600 K, and the adsorption of CO_2 was proposed as being reversible in this temperature range (*15*). These observations are consistent with an increase in u_{CO_2} between 453 and 523 K. (c) Nonequilibrium conditions exist, in which adsorption is irreversible and/or an additional surface reaction takes place (e.g., carbon deposition, nickel carbide formation, surface oxidation). In this case, even if the adsorption system is at true steady state, an increase in temperature will cause an increase in the rate of irreversible adsorption, an increase in surface utilization, and therefore, an increase in u_i. The adsorptions of CO, CH_4, and CO_2 fall into this category. For temperatures above 300 K, the adsorptions of CO and CH_4 are irreversible; they are accompanied by carbon deposition via the Boudouard reaction (*16, 17*), and nickel carbide formation via dehydrogenative adsorption (*18, 19*), for CO and CH_4, respectively. Carbon dioxide also adsorbs irreversibly above 523 K, apparently as a result of its dissociation into CO and O surface species (*20, 21*). Thus, surface utilization coefficients for CO, CH_4, and CO_2 are expected to increase with temperature.

Comparison of surface utilization for the products (CH_4 and H_2O) with that of the reactants suggests that inhibition by the former cannot be neglected. Previous studies of Ni-catalyzed methanation reactions typically ignored product inhibition; this is probably due to low conversions. In a recent study of the nickel-catalyzed shift-methanation reaction (CO + H_2O), the adsorption of H_2O alone, and with CO, on an alumina-supported Ni catalyst, was investigated using IR spectroscopy (*22*). It was concluded that H_2O dissociatively adsorbed on the Ni surface (in addition to the support material), at temperatures above 300 K, and that its presence on the surface played an active role in the methanation reaction mechanism.

Each of the adsorbates studied in the present work have been previously investigated for their adsorption behavior on Ni/SiO_2 catalysts. Adsorption studies with application of the low-field magnetic-induction method, have successfully used the procedures developed by Selwood (*2*) for correlating magnetization–adsorption data. However, these studies mostly employed vacuum conditions, and quantitative correlations were performed for H_2 and O_2 only (*23–25*). In a study of sulfiding in nickel catalyst beds (*26*), magnetic output vs bed depth data were successfully correlated with a polynomial equation.

Kinetic Modeling

Reaction rate expressions employed for the carbon oxide hydrogenations are of the Langmuir–Hinshelwood form. Success of correlating the magnetic-adsorption data with a Langmuir type of equation suggests that the hydrogenation rate data can be modeled in a similar way. The justification for this functional form is that it is consistent with the kinetic data, and can be used for interrelating the surface utilization coefficients in a relatively simple way. The approach taken in this work is to use the surface utilization coefficients, u_i, of the single-species studies in the rate equations and to determine the reaction velocity from the kinetic data. The relative magnitudes of the u_i reflect the relative strengths of interaction with the nickel surface. Clearly, adsorption behavior under hydrogenation conditions is expected to differ from the single-species study; nevertheless, inclusion of the various u_i in the rate expressions serves as a practical approximation in modeling the data.

Similar to the single-species adsorption analysis, the surface utilization function for multicomponent adsorption is expected to be of the form

$$\frac{U_i}{S_i} = \frac{u_i P_i}{1 + \sum_j u_j P_j}, \qquad (18)$$

where the summation is performed for all the adsorbates present during reaction conditions. Using the *principle of mass action*

between reacting species, the rate of methanation is made to be proportional to the product of the surface utilization ratios of hydrogen and the carbon oxide,

$$r_{CH_4} = k_0(U_{H_2}/S_{H_2})(U_{CO_x}/S_{CO_x}) \quad (19)$$

or

$$r_{CH_4} = k_0 \frac{(u_{H_2}P_{H_2})(u_{CO_x}O_{CO_x})}{[1 + (u_{H_2}P_{H_2}) + (u_{CO_x}P_{CO_x}) + (u_{CH_4}P_{CH_4}) + (u_{H_2O}P_{H_2O})]^2}. \quad (20)$$

This generalized rate equation contains just one adjustable parameter, k_0. Analysis of the adsorption data showed that surface utilization by CH_4 is not necessarily negligible, as $u_{CH_4} \gg u_{CO_x}$ (Table 2). Most methanation conditions used in this study favored significant conversions to CH_4; thus, neglecting the inhibition effect by these species in the rate equations is not justified. This is a practice favored by most studies of carbon oxide hydrogenations. To show this effect on the kinetic modeling, two forms of the rate equation, one including terms for CH_4 and H_2O in Eq. (20), and another in which $u_{CH_4} = u_{H_2O} = 0$, were applied (the two forms are denoted by (+) and (−), respectively in the following discussion).

Since conversion was not small, an isothermal plug-flow reactor is assumed. The longitudinal thermal gradient, across the catalyst bed, during reaction conditions, was less than 5° (*9*). This result was used as the main criterion for reactor isothermality. A steady-state material balance for any species i over a differential mass of catalyst gives $r_i = dF_i/dW$, where r_i is the net rate of formation of i by chemical reaction (mol i/h g-catalyst), F_i is the molar flow rate of i (mol i/h), and W is the mass of catalyst in the reactor (g). Since the reaction mixtures were always over 95% hydrogen, negligible change in the total molar flow rate, F, is assumed and thus, $F_i = (P_i/P_{total})F$. The yield based on amount of carbon oxide fed to the reactor is defined as

$$Y = \frac{\nu_{CO_x}}{\nu_i}\left(\frac{P_i^0 - P_i}{P_{CO_x}^0}\right), \quad (21)$$

where the P_i^0 are the feed partial pressures, and the ν_i are the stoichiometric coefficients (positive for products). The rate of methane formation can thus be written as

$$r_{CH_4} = \frac{dY}{d(W/F_{CO_x}^0)}. \quad (22)$$

Substituting Eq. (20) into Eq. (22) results in an expression which can readily be integrated, using the linear relationship between the P_i and $P_{CO_x}^0$; the rate constant, k_0, is readily determined.

Good description of CH_4 yield is obtained for both carbon oxide methanations, by either form of the rate equation. The rate equation incorporating product inhibition (form +), gave a slightly better fit to the data, and was used to calculate CH_4 yields. These are compared with the experimental data in Figs. 4 and 5 (curves in upper part). Arrhenius plots of the rate constants (Fig. 11) show deviation from linearity in the high-temperature region (>493 K). This is especially evident for the (−) form of CO_2 methanation. Product inhibition effect is noticeable in that reaction, while it is almost negligible for CO methanation.

The model can now be put to the ultimate test by comparing the predicted change in $\Delta M/M$, under reaction conditions, with the experimental values. To that end we assume that the total magnetic loss is a simple sum of the individual contributions

$$\left(\frac{\Delta M}{M}\right)_{total} = \frac{1}{(W/F_{CO_x}^0)} \int \sum_i \left(\frac{\Delta M}{M}\right)_i d(W/F_{CO_x}^0), \quad (23)$$

where to a first-order approximation

$$\sum_i \left(\frac{\Delta M}{M}\right)_i = \sum_i \frac{-2C_m S_i u_i P_i}{1 + \sum_j u_j P_j}. \quad (24)$$

The quadratic contribution in Eq. (16) is ne-

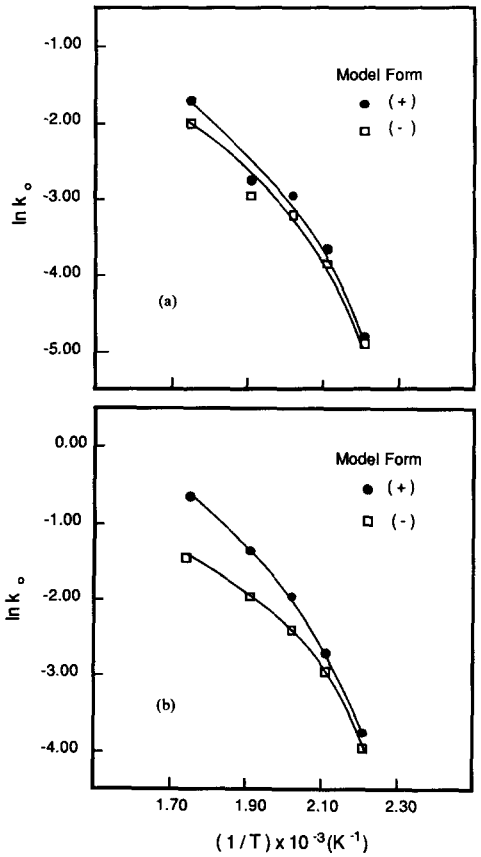

FIG. 11. Arrhenius plots of the rate constants of the proposed kinetic model for CO (a), and for CO_2 (b) methanation reactions.

glected, which is a justified assumption for most of our data. The integration of Eq. (23) is an averaging process over the reactor, which is necessary when the yield (or conversion) is significant. Substitution of Eq. (22) for $d(W/F^0_{CO_x})$, along with Eqs. (20) and (24), into Eq. (23), results in

$$\left(\frac{\Delta M}{M}\right)_{\text{total}} = \frac{1}{(W/F^0_{CO_x})} \int \frac{\left(\sum_i -2C_m S_i u_i P_i\right)\left(1 + \sum_j u_j P_j\right)}{k_0 (u_{H_2} P_{H_2})(u_{CO_x} P_{CO_x})} dY. \quad (25)$$

The integral can be solved analytically and $(\Delta M/M)$ can be estimated using the predetermined values of the u_i (Table 2), and k_0 (Fig. 11); note that k_0 will have a minor effect on the computation if the yield is sufficiently small. The data presented in Figs. 4 and 5 represent the magnetic loss from a reference of a surface initially exposed to H_2, thus

$$\left(\frac{\Delta M}{M}\right) = \left(\frac{\Delta M}{M}\right)_{\text{total}} + \frac{2C_m S_{H_2} P^0_{H_2}}{1 + U_{H_2} P^0_{H_2}}. \quad (26)$$

Predicted relative magnetic losses are compared to the experimental values at three temperatures (Fig. 12). A reasonable fit to the magnetic data is obtained for CO_2 methanation. For CO methanation, the predicted magnetic losses ascend with increasing temperature, contrary to experimental observation. Consequently, a significant deviation between the calculated and experimental values exists at the higher tempera-

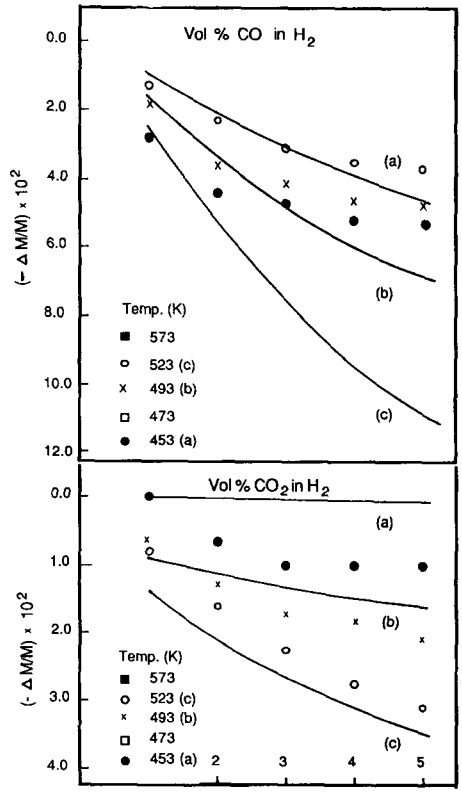

FIG. 12. Observed and predicted relative magnetic losses for CO and CO_2 methanations (curves correspond to Eq. 26).

tures (>493 K). This effect is due to irreversible adsorption and catalyst deactivation (carbon deposition). These irreversible processes accelerate with temperature during the single-species adsorption, and u_{CO} and u_{CH_4} reflect that trend. Under reaction conditions, however, irreversibly adsorbed species apparently react with hydrogen, and this effect is of smaller magnitude or entirely nonexistent.

CONCLUSIONS

Under the conditions studied, adsorbed CO and CH_4 are the dominant surface species during the methanations of CO and CO_2, respectively. The results strongly suggest that each carbon oxide methanation reaction procedes by a different surface mechanism.

Mathematical models acquire a higher credibility with fewer adjustable parameters. Ultimately, a model should yield good description of a process when all of its parameters are estimated independently. In predicting catalytic reaction rates, adsorption parameters should be estimated independently, leaving only the rate constant to be fitted. This procedure yields good description of the rate for both methanation reactions studied here. The magnetic loss during reaction conditions can be calculated with predetermined parameters and no adjustable constant. The total magnetic loss during methanation is assumed to be a simple sum of the individual contributions. Adequate approximation is obtained for CO_2 methanation, whereas, significant deviation exists for CO methanation. The latter result is due to the falsification of CO and possibly CH_4 adsorption parameters by irreversible processes.

The low-field magnetic induction method has been shown to be useful for investigating the *in situ* surface behavior of CO and CO_2 methanation reactions, at practical reactor conditions. Results of the adsorption experiments gave *in situ* information on the surface behavior of the individual reactants, which was pivotal for interpreting the results of the methanation reactions.

APPENDIX: NOMENCLATURE

BET	Brunauer-Emmett-Teller (adsorption equation).
C_m	magnetic coefficient defined by Eqn. (8).
F	total molar flow rate entering the reactor.
F_i	molar flow rate of species i.
$F^0_{CO^x}$	initial molar flow rate of the carbon oxide.
g_i	total number of molecules adsorbed.
H	applied magnetic field.
I_s	spontaneous magnetization.
k	Boltzmann constant.
k_0	reaction rate constant.
M	catalyst magnetization.
m_i	change in magnetic moment per particle.
N	number of catalyst particles.
n_B	number of Bohr magnetons per nickel atom.
P_i	partial pressure of component i.
P_i^0	initial partial pressure of component i.
P_{total}	total reactor pressure.
r_i	rate of reaction based on reactant i.
S_i	maximum site number for molecule i.
s_i	bond number for molecule i.
T, T_i	temperature.
T_r	reference temperature.
U_i	surface utilization function for adsorbate i.
u_i	surface utilization coefficient for adsorbate i.
V_p	total volume of catalyst particles.
v_p	particle volume.
W	catalyst weight.
x_i	number of molecules adsorbed per catalyst particle.

Y	reaction yield.
ΔM	change in catalyst magnetization.
$\frac{\Delta M}{M}$	relative change in catalyst magnetization.
Δt	change in time.
$\gamma(T_i, T_r)$	relative magnetic moment.
$\Delta\mu$	change in dipole magnetic moment.
μ_B	Bohr magneton.
ν_i	stoichiometric coefficient.

REFERENCES

1. Bean, C. P., and Livingston, J. D., *J. Appl. Phys.* **30,** 120S (1959).
2. Selwood, P. W., "Adsorption and Collective Paramagnetism." Academic Press, New York (1962).
3. Van Meerten, R. Z. C., Beaumont, A. H. G. M., Van Nisselrooij, P. F. M. T., and Coenen, J. W. E., *Surf. Sci.* **135,** 565 (1983).
4. Van Meerten, R. Z. C., De Graaf, T. F. M., and Coenen, J. W. E., *J. Catal.* **46,** 1 (1977).
5. Dalmon, J. A., and Martin, G. A., *J. Catal.* **84,** 45 (1983).
6. Dalmon, J. A., and Martin, G. A., *J. Chem. Soc., Fararaday Trans. I* **75,** 1011 (1979).
7. Cale, T. S., *J. Catal.* **90,** 40 (1984).
8. Anderson, J. R., and Pratt, K. C., "Introduction to Characterization and Testing of Catalysts." Academic Press, Sydney (1985).
9. Yesgar, P. W., D. Sc. dissertation, Technion-IIT, Israel (1988).
10. Cale, T. S., Richardson, J. T., and Ginestra, J., *Appl. Phys. Lett.* **42**(8), 1983.
11. Chen, Chih-wen, "Magnetism and Metallurgy of Soft Magnetic Materials." North-Holland Pub. Co., Amsterdam (1977).
12. Falconer, J. L., and Zagli, A. E., *J. Catal.* **62,** 280 (1980).
13. Martin, G. A., Imelik, B., *Surf. Sci.* **42,** 157 (1974).
14. Paal, Z. and Menon, P. G., Eds., "Hydrogen effects in Catalysis." Dekker, New York (1988).
15. Martin, G. A., Primet, M., and Dalmon, J. A., *J. Catal.* **53,** 321 (1978).
16. Kuijpers, E. G. M., Kock, A. J. H., Nieuwesteeg, C. M. A., and Geus, J. W., *J. Catal.* **95,** 13 (1985).
17. Blackmond, D. G., and Ko, E. I., *J. Catal.* **96,** 210 (1985).
18. Kuijpers, E. G. M., Breedijk, A. K., Van Der Wal, W. J. J., and Geus, J. W., *J. Catal.* **81,** 429 (1983).
19. Kuijpers, E. G. M., Breedijk, A. K., Van Der Wal, W. J. J., and Geus, J. W., *J. Catal.* **72,** 75 (1981).
20. D'evelyn, M. P., Hamza, A. V., Gdowski, G. E., and Madix, R. J., *Surf. Sci.* **167,** 451 (1986).
21. Falconer, J. L., and Zagli, A. E., *J. Catal.* **62,** 280 (1980).
22. Yilu, F., Xiqing, L., and Xiaoyun, X., *Appl. Catal.* **25,** 27 (1986).
23. Van Meerten, R. Z. C., De Graaf, T. F. M., and Coenen, J. W. E., *J. Catal.* **46,** 1 (1977).
24. Martin, G. A., De Mongolfier, P., and Imelik, B., *Surf. Sci.* **3,** 675 (1973).
25. Geus, J. W., and Nobel, A. P. P., *J. Catal.* **6,** 108 (1966).
26. Richardson, J. T., *J. Catal.* **21,** 130 (1971).